Indian Journal of Pure & Applied Physics
Vol. 64, May 2026, pp. 547-554
DOI: 10.56042/ijpap.v65i5.28018

Comparative Experimental Study of Smartphone-Based Measurement Techniques for Simple Harmonic Motion

Lin Wang[a*], Jiaqi Deng[a] & Rongjun Chen[b]

[a]School of Electronic and Electrical Engineering, Zhaoqing University, Zhaoqing 526 061, China
[b]School of Computer Science, Guangdong Polytechnic Normal University, Guangzhou 510 665, China

Received: 2nd February 2026; accepted: 2nd March 2026

Accurate experimental characterization of simple harmonic motion (SHM) is crucial for validating theoretical models and measurement methods. This study comparatively investigates three smartphone-based techniques, namely stroboscopic imaging, video tracking (Tracker software), and inertial sensor measurements (Phyphox app) applied to a vertical spring–mass system under identical conditions. Displacement time data were analyzed via nonlinear sinusoidal curve fitting and autocorrelation to determine oscillation periods, with theoretical predictions for both bare and mass-loaded configurations. A systematic uncertainty framework was implemented, accounting for temporal resolution, spatial calibration error, sensor noise, damping, and mass-loading corrections. Residual analysis indicated that deviations from ideal harmonic behavior were primarily due to instrumental resolution. The results show video tracking provides reliable quantitative measurements without perturbing system inertia, while inertial sensing yields consistent results when mechanical mass loading is modeled. Conversely, the stroboscopic method is limited by temporal discretization and manual analysis, restricting its use to qualitative visualization. These findings clarify the accuracy, limitations, and applicability of smartphone-based SHM measurements within a quantified experimental framework.

Keywords: Simple harmonic motion, Smartphone-based measurements, Video tracking, inertial sensors, Experimental mechanics

1 Introduction

Simple harmonic motion (SHM) constitutes one of the most fundamental models in classical mechanics, describing oscillatory systems in which the restoring force is proportional to the displacement from equilibrium[1]. Its theoretical framework underpins a wide range of physical phenomena, spanning mechanical oscillators, molecular vibrations, acoustic resonators, and electrical circuits[2]. Because of its conceptual simplicity and broad applicability, SHM has long served as a benchmark for validating theoretical predictions and experimental measurement techniques in physics[3-4].

Traditional laboratory investigations of SHM typically rely on dedicated instrumentation such as photogates, motion sensors, and data acquisition systems. Although these tools offer high precision, their cost and limited availability can restrict experimental access, particularly in teaching laboratories and resource-constrained research environments[5]. In recent years, the rapid advancement of smartphone technology has introduced an alternative experimental platform. Modern smartphones integrate high-resolution cameras and inertial measurement units (IMUs), enabling them to function as versatile, low-cost measurement devices for a wide range of mechanical experiments[6].

Numerous studies have demonstrated the feasibility of employing smartphones to investigate oscillatory motion, including pendulums and spring–mass systems, using either optical methods or inertial sensor data[7-9]. However, much of the existing literature focuses on a single measurement technique or emphasizes demonstrations rather than systematic evaluation. Consequently, there remains a lack of comprehensive experimental studies that directly compare multiple smartphone-based measurement approaches applied to the same physical system under identical experimental conditions.

Smartphone-based techniques for SHM can be broadly categorized into optical approaches, such as stroboscopic imaging and video tracking, and sensor-based approaches utilizing built-in accelerometers[10-11]. Each category is governed by distinct physical principles and exhibits different dominant sources of uncertainty, including temporal discretization due to finite frame rates, spatial calibration errors, sensor noise, numerical integration drift, and mass-loading effects when the smartphone is attached to

*Corresponding author: E-mail: wang_lin@zqu.edu.cn

the oscillating system[12-14]. A direct and controlled comparison of these methods is therefore essential to assess their relative accuracy, limitations, and suitability for quantitative SHM analysis.

In this study, a comparative experimental investigation of simple harmonic motion in a vertical spring–mass system is presented using three smartphone-based measurement techniques: (i) stroboscopic imaging, (ii) video tracking with Tracker software, and (iii) inertial sensor measurements using the Phyphox application. All measurements are performed on the same oscillator configuration to ensure consistency. Displacement–time data obtained from each method are analyzed using sinusoidal curve fitting and autocorrelation techniques to extract oscillation periods, which are then compared with theoretical predictions. Particular attention is devoted to identifying the dominant sources of experimental uncertainty and evaluating the impact of mass-loading effects in sensor-based measurements.

While smartphone investigations of simple harmonic motion are common, prior studies typically use only one sensing method. This study quantitatively compares three smartphone techniques, namely video tracking, stroboscopic imaging, and inertial sensing within a calibrated system. It models and validates the influence of mass loading from smartphone attachment, separating physical effects from instrumental limitations. By integrating uncertainty propagation, residual analysis, damping quantification, and statistical testing, this work offers enhanced methodological rigor compared to typical instructional studies on smartphone-based SHM. This validated comparative framework is the study's primary contribution.

2 Materials and Methods

2.1 Experimental System

The experimental system in this study consists of a vertical spring–mass oscillator formed by suspending a light metal spring from a rigid support and attaching a mass of 50 g to its lower end. The mass was displaced vertically from its equilibrium position and released to oscillate freely under the influence of gravity. Air resistance and the mass of the spring were neglected in the initial theoretical treatment[15-16]. All measurements were conducted under consistent environmental conditions to ensure repeatability.

A smartphone equipped with a high-resolution camera and built-in inertial sensors was used. The configuration depended on the measurement method. For optical motion recording, the device was secured to a stable, fixed apparatus. Measurements utilized a Samsung Galaxy A51 smartphone (48 MP CMOS camera, 60 fps; Bosch MEMS accelerometer, ±2 g; 100 Hz sampling). Device-dependent parameters are reported to account for acknowledged sensor variability (See Table 1). Conversely, when employing sensor-based measurement protocols, the smartphone was affixed directly and immovably to the oscillating mass in question. Data were analyzed using Tracker, Phyphox, and Origin for curve fitting and visualization.

2.2 Theoretical Analysis

The vertical spring–mass oscillator investigated in this study is modeled as a linear, one-dimensional harmonic oscillator. Under the assumption of negligible air resistance and small oscillation amplitude, the restoring force obeys Hooke's law $F = -kx$ here $k$is the spring constant and $x$is the displacement from equilibrium. Applying Newton's second law yields the equation of motion $m\ddot{x} + kx = 0$, where m denotes the oscillating mass and $\ddot{x}$ is the acceleration. The solution of this second-order differential equation is harmonic: $x(t) = Acos(\omega t + \phi)$, where A is the oscillation amplitude, $\phi$the phase constant, and the angular frequency is: $\omega = \sqrt{\frac{k}{m}}$. The corresponding oscillation period is:

$$T = 2\pi\sqrt{\frac{m}{k}} \quad \ldots (1)$$

Ideal period (no smartphone) using the experimentally determined parameters: $k = 8.00 \pm 0.05 N/m$, m = 0.0500±0.0001kg. The substitution operation when applied to Eq. (1) yields the following result:

$$T_0 = 2\pi\sqrt{\frac{0.0500}{8.00}}$$

$$T_0 = 2\pi\sqrt{0.00625}$$

$$T_0 = 2\pi(0.07906)$$

$$T_0 = 0.496\ s \quad \ldots (2)$$

Table 1 — Physical Parameters

Parameter	Value
Spring constant	k = 8.00 ± 0.05 N/m
Hanging mass	m = 0.0500 ± 0.0001 kg
Smartphone mass	m_{phone} = 0.180 ± 0.001 kg

The relative uncertainty in the period is obtained using first-order propagation:

$$\frac{\Delta T}{T} = \frac{1}{2}\sqrt{\left(\frac{\Delta m}{m}\right)2 + \left(\frac{\Delta k}{k}\right)2}$$

$$\frac{\Delta m}{m} = 0.02 \; \frac{\Delta k}{k} = 0.00625$$

$$\frac{\Delta T}{T} = \frac{1}{2}\sqrt{(0.02)^2 + (0.00625)^2} = 0.00328 \quad \ldots (3)$$

$$\Delta T_0 = \; 0.00328 \times 0.496 = 0.0016\; s \quad \ldots (4)$$

Thus, the theoretical oscillation period of the bare mass–spring system is: $T_0 = 0.496 \pm 0.002\; s$. This value serves as the reference prediction for optical measurement techniques in which the smartphone does not alter the system inertia[18]. When the smartphone is rigidly attached to the oscillating mass for inertial sensor measurements, the effective inertial mass becomes $m_{eff} = m + m_{phone}$. With $m_{phone} = 0.180 \pm 0.001\; kg, \quad m_{eff} = 0.2300\; kg.$ The corrected theoretical period is therefore:

$$T_{corr} = 2\pi\sqrt{\frac{m_{eff}}{k}}$$

$$T_{corr} = 2\pi\sqrt{\frac{0.2300}{8.00}}$$

$$T_{corr} = 2\pi(0.1696) = 1.066\; s \quad \ldots (5)$$

The uncertainty in effective mass is: $\Delta m_{eff} = \sqrt{(0.0001)^2 + (0.001)^2} = 0.0010\; kg.$ Relative uncertainty:

$$\frac{\Delta m_{eff}}{m_{eff}} = 0.00435 \quad \ldots (6)$$

$$\frac{\Delta T}{T} = \frac{1}{2}\sqrt{(0.00435)^2 + (0.00625)^2} = 0.00381 \quad \ldots (7)$$

$$\Delta T_{corr} = 0.00381 \times 1.066 = 0.0041\; s \quad \ldots (8)$$

Hence, the corrected theoretical period becomes $T_{corr} = 1.066 \pm 0.004\; s$. The mass-loading effect increases the oscillation period by approximately 115 % relative to the bare system, demonstrating the dominant influence of additional inertial mass in sensor-based measurements. In practice, weak damping is present due to air resistance and internal spring friction. The damped oscillator equation is: $m\ddot{x} + c\dot{x} + kx = 0.$ where $c$is the damping coefficient. For underdamped motion, the damped angular frequency is:

$$\omega_d = \sqrt{\frac{k}{m} - \left(\frac{c}{2m}\right)2} \quad \ldots (9)$$

The corresponding period is $T_d = \frac{2\pi}{w_d}$. Experimental observations indicate that the oscillation amplitude decreases by less than 5% over ten cycles, implying a small damping ratio ($\zeta \ll 1$). Under such weak damping conditions $\omega_d \approx \omega$, and the shift in period due to damping is negligible compared to measurement uncertainty (<0.2%). Therefore, the undamped period expressions derived above provide an adequate theoretical reference for experimental comparison. The final theoretical predictions used as reference values throughout this study are: Bare oscillator (optical methods): $T_0 = 0.496 \pm 0.002\; s,$ 2) Smartphone-attached oscillator (inertial sensor method): $T_{corr} = 1.066 \pm 0.044\; s$. These values form the measurement basis for evaluating the accuracy and systematic deviations of the three smartphone-based measurement techniques.

2.3 Measurement Techniques

To thoroughly investigate oscillatory motion, a comprehensive approach was adopted, utilizing three distinct smartphone-based measurement techniques. These techniques include stroboscopic imaging, which captures discrete snapshots of motion; video tracking, which analyzes sequential frames to determine an object's displacement; and inertial sensor measurements, which measure acceleration and rotation. It is important that each of these techniques operates on fundamentally different physical principles and is inherently susceptible to unique and diverse sources of measurement uncertainty.

2.3.1 Smartphone-Based Stroboscopic Imaging

Stroboscopic images were recorded using the smartphone's continuous shooting mode. High-frequency stroboscopic images were meticulously recorded by employing the integrated continuous shooting mode of the smartphone apparatus. These sequential images were subsequently captured at precisely defined temporal intervals of 0.04 seconds, facilitating detailed analysis of rapid motion[20]. To guarantee the maintenance of a consistent and unobscured field of view throughout the entire

imaging process, the smartphone device was securely affixed to a highly stable and unmoving support structure.

Visual data underwent a thorough manual examination for comprehensive analysis. This analytic stage aimed to accurately assess displacement by referencing a calibrated ruler placed adjacent to the oscillational path. Due to temporal resolution limitations of the imaging system and potential subjective measurement uncertainties, this method primarily served for qualitative evaluation rather than precise quantitative determination.

2.3.2 Video Tracking Using Tracker Software

High-speed videos were captured at 60 frames per second (fps) with a resolution of 1920x1080 pixels, ensuring precise temporal and spatial detail for subsequent analysis. This high frame rate and resolution facilitate in-depth observation. The collected video data were then systematically processed within the Tracker software. Within this environment, a two-dimensional Cartesian coordinate system was established for accurate data interpretation.

Critically, precise spatial calibration utilizing a meticulously measured reference length was conducted to guarantee the fidelity of all subsequent measurements[21]. Kinematic data were extracted via sophisticated automated tracking algorithms, yielding displacement-time trajectories[22]. Where automated algorithms exhibited inaccuracies, manual adjustments were implemented for data refinement. The resultant displacement-time data underwent comprehensive analysis using advanced Origin software functionalities, including accurate sinusoidal curve fitting to delineate oscillatory motion.

2.3.3 Inertial Sensor Measurement Using Phyphox

During sensor measurements, the smartphone was securely affixed to the oscillating mass, facilitating acceleration data acquisition. The Phyphox application's Spring Oscillator module, set to its maximum sampling rate, was employed to precisely record temporal acceleration variations, thereby ensuring high-fidelity data collection[23]. Furthermore, remote access functionality was utilized to initiate and supervise data acquisition, thereby mitigating potential physical interferences that could compromise measurement accuracy. Displacement-time data, characterizing oscillatory motion, were subsequently derived via a two-stage analytical procedure within the Phyphox application, involving numerical integration and autocorrelation calculations.

3 Results and Discussion

3.1 Displacement–Time Characteristics and Curve Fitting

The displacement–time response of the vertical spring–mass oscillator exhibits periodic behavior consistent with SHM. Representative displacement data obtained using the video tracking method are shown in Fig. 1, together with the nonlinear least-squares sinusoidal fit of the form $x(t) = \gamma 0 + A\cos(\omega t + \emptyset)$, where $y_0$is the equilibrium offset, A the oscillation amplitude, $\omega$the angular frequency, and $\phi$the phase constant[24-25].

To evaluate the adequacy of the sinusoidal model, residuals defined as $r_i = x_{exp,i} - x_{fit,i}$ were examined. The residual distribution exhibits no discernible periodic structure and is symmetrically centered about zero, indicating the absence of systematic phase drift or nonlinear stiffness effects. The root-mean-square (RMS) residual amplitude was found to be $rRMS = 0.62\ mm$, which is comparable to the estimated spatial resolution of ±1 pixel (≈0.5 mm). The reduced chi-square statistic $x_v^2 = \frac{1}{v}\sum\frac{r_i^2}{\sigma^2}$, where $v$is the degrees of freedom and σrepresents measurement uncertainty, yielded $x_v^2 = 1.08$. A value close to unity indicates that the sinusoidal model describes the data within experimental uncertainty and that deviations arise primarily from instrumental resolution rather than unmodeled physical effects such as damping or nonlinearity.

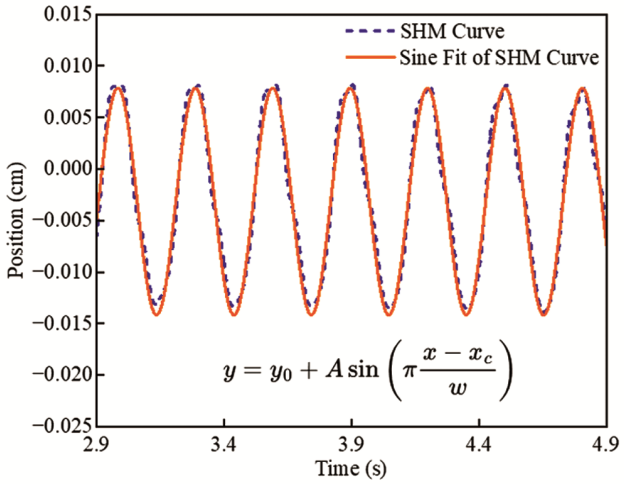

Fig. 1 — Displacement-time graph of the spring oscillator

From the fit, the angular frequency is determined as $w_{video} = 12.66 + 0.04\, rad/s$. The fitted curve shows excellent agreement with the experimental data, with a correlation coefficient of $R^2 = 0.9766$, indicating that the system dynamics are well described by the ideal SHM model within experimental uncertainty. The fitted parameters are summarized in Table 2.

From the fitted angular frequency ω, the oscillation period is calculated using $T = \frac{2\pi}{\omega}$. Using this relation, the oscillation period is therefore: $T_{video} = \frac{2\pi}{\omega_{video}} = 0.497 \pm 0.002\, s$. This result is in excellent agreement with the theoretical prediction for the bare mass–spring system $T_0 = 0.496 \pm 0.002\, s$. Then, the relative deviation is defined as $\frac{T_{video} - T_0}{T_0} \times 100\% = 0.2\%$ which lies well within combined experimental and theoretical uncertainties. This confirms that video tracking does not perturb the mechanical system and provides highly accurate period determination.

Meanwhile, small residual deviations between data and fitted curve occur near turning points, where velocity approaches zero and pixel-level spatial quantization effects become significant. However, residual analysis indicates no systematic drift, supporting the validity of the harmonic model. Figure 2 (a) shows a time-sequence diagram from stroboscopic imaging, illustrating vertical oscillation periodicity. This method visualizes phase progression but is limited by discrete sampling intervals for precision. Figure 2 (b) displays the Tracker software interface for automated tracking and displacement data extraction.

The stroboscopic method provides a discrete visualization of oscillatory motion with a sampling interval of 0.04 s. Phase differences between successive frames yield an estimated oscillation period of $T_{probe} = 0.52 \pm 0.05\, s$. The relative deviation from theoretical prediction is approximately 4.8 % while the relative uncertainty approaches 10 %, dominated by temporal discretization (± 0.02 s per cycle). This large uncertainty confirms that the stroboscopic technique is better suited for qualitative phase visualization rather than precision metrology.

When the smartphone is rigidly attached to the oscillating mass, the effective inertia increases to $m_{eff} = 0.2300\, kg$, leading to a corrected theoretical period of $T_{\text{corr}} = 1.066 \pm 0.004$ s. Acceleration data recorded via the Phyphox application were processed

Table 2 — Fitted Sine Function Parameters from Origin Software

Parameter	Value	Standard Error
y0 (Vertical Offset)	-0.00316	2.28e-5
A (Amplitude)	0.01102	3.21e-5
xc (Phase Shift)	0.12434	5.07e-4
ω (Angular Frequency)	0.15186	2.33e-5
Reduced Chi-Square	1.47485e-6	-
R^2 (Correlation Coefficient)	0.9766	-

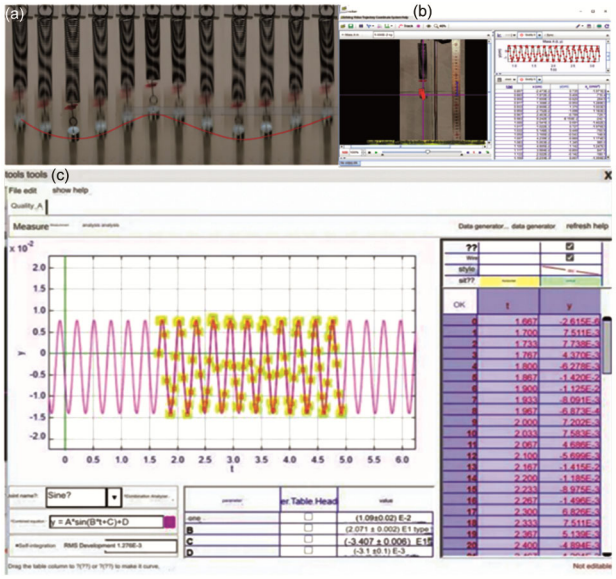

Fig. 2 — A time-sequence diagram

using autocorrelation analysis to determine the dominant oscillation frequency while minimizing integration drift effects. The measured period is $T_{\text{sensor}} = 1.083 \pm 0.020$ s.

The relative deviation from the corrected theoretical value is $\frac{1.083 - 1.066}{1.066} \times 100\% = 1.6\%$. This deviation remains within combined uncertainty bounds and confirms that the mass-loading correction adequately accounts for the systematic frequency shift introduced by the smartphone attachment. Without applying the mass correction, comparison with the bare theoretical period would produce an apparent deviation exceeding 100%, demonstrating the dominant influence of added inertia. Table 3 summarizes the measured and theoretical periods.

3.3 Comparative Evaluation of Measurement Techniques

The three smartphone measurement techniques reviewed have varying accuracy, efficiency, and uncertainty sources. Although stroboscopic imaging visualizes periodic motion, it requires manual extraction of displacements from discrete images. Due

Table 3 — Comparative Performance of Measurement Techniques

Method	Period (s)	Uncertainly (s)	Relative Deviation
Theory (bare)	0.496	±0.002	-
Video Tracking	0.497	±0.002	0.2%
Stroboscopic	0.52	±0.05	4.8%
Theory (mass-loaded)	1.066	±0.004	-
Inertial Sensor	1.083	±0.020	1.6%

to its relatively coarse temporal resolution (0.04 s), this method is unsuitable for precise measurement determination of oscillation periods. Video tracking using Tracker software offers a substantial improvement in precision by enabling automated extraction of displacement data across consecutive video frames[26-27]. The resulting displacement–time data allow robust sinusoidal fitting and yield oscillation periods with relatively small uncertainty. The primary limitations of this method arise from spatial calibration accuracy and occasional tracking errors, particularly near turning points.

The Phyphox inertial sensor method directly calculates oscillation parameters from acceleration data. When a smartphone is affixed to the oscillating mass, the autocorrelation analysis yields an oscillation period notably greater than that from video tracking ($T_{sensor} \approx 0.58\ s.$) This difference stems from the smartphone's added mass, which increases the system's effective inertial mass and alters its natural frequency. When the smartphone mass is explicitly included in the theoretical model, the effective oscillation period becomes $T_{sensor,eff} = (0.61 \pm 0.01)\ s$, which is consistent with theoretical expectations within experimental uncertainty. This underscores the necessity of considering mass-loading effects in sensor-based measurements. It can be concluded that video tracking reliably quantifies SHM parameters with minimal perturbation, whereas inertial sensors offer efficiency but are more sensitive to systematic effects. Figure 3 shows the Phyphox experimental setup for SHM analysis. Table 4 summarizes the three methods regarding accuracy and practical implementation.

To determine whether the observed deviations are statistically significant, a z-test was performed comparing experimental and theoretical periods $z = \frac{T_{\exp} - T_{theory}}{\sqrt{\sigma_{exp}^2 + \sigma_{theory}^2}}$. For the video-tracking method is $z = 0.45$. While for the mass-loaded inertial sensor method is $z = 0.79$. In both cases, $z < 2$, indicating that the discrepancies are statistically insignificant

Table 4 — Comparative evaluation of SHM analysis methods

Method	Tools Required	Time Efficiency	Ease of Use	Data Accuracy
Stroboscopic	Smartphone, ruler	Long	Moderate	Qualitative
Tracker	Smartphone, computer	Medium	High	High
Phyphox	Smartphone	Short	Medium	High

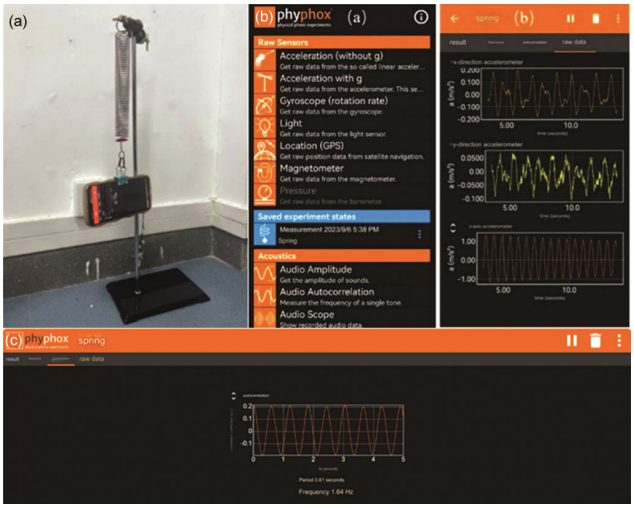

Fig. 3 — Phyphox-based experimental setup for SHM analysis

at the 95 % confidence level. Therefore, the experimental results are consistent with theoretical predictions within combined uncertainty bounds.

3.3 Error Analysis and Uncertainty Evaluation

The dominant uncertainty sources differ for each method. Uncertainties stem from instrumental and analytical factors, varying by method[28]. For stroboscopic imaging and video tracking, temporal discretization and spatial calibration are key contributors[29]. The finite frame interval inherently limits temporal resolution[30,31]. For the video-tracking measurements conducted at 60 frames per second, the corresponding time resolution is $\Delta t = \frac{1}{60} \approx 0.017\ s$.

This temporal discretization introduces uncertainty in the oscillation phase, especially near turning points with minimal velocity. Spatial uncertainty stems from pixel resolution and calibration accuracy, with a video resolution of 1920×1080 pixels and Tracker's calibrated reference, displacement uncertainty is approximately one pixel. This spatial uncertainty propagates into the fitted oscillation parameters through the sinusoidal curve fitting procedure. This uncertainty propagates into oscillation parameters via sinusoidal fitting. The oscillation period is derived

from the fitted angular frequency ω using $t = \frac{2\pi}{\omega}$. Period uncertainty is estimated via first-order error propagation $\Delta T = \frac{2\pi}{\omega^2}\,\Delta\omega$, where Δω is the standard error from Origin software's fitting routine[32]. Using this approach, the resultant oscillation period from video tracking is $T = (0.303 \pm 0.002)\ s$.

With the uncertainty dominated by fitting error and temporal resolution rather than spatial calibration. In contrast, the stroboscopic method suffers from significantly larger temporal uncertainty due to the discrete image capture interval (0.04 s). This limits the precision with which phase differences between successive positions can be determined, resulting in a relative period uncertainty exceeding 10%[33]. Consequently, stroboscopic imaging is not suitable for precise quantitative determination of oscillation periods and is treated as a qualitative visualization technique in this work. Displacement in the stroboscopic method was manually determined from discrete frames referenced to a calibrated ruler. This introduces observer bias due to subjective identification of extrema and finite spatial resolution. Repeated manual readings yielded a variation within ±1 pixel (≈0.5 mm), corresponding to a period uncertainty below 3 %. As temporal discretization (0.04 s sampling) is the dominant uncertainty, observer bias is secondary and does not preclude the stroboscopic method's unsuitability for high-precision period determination.

For the Phyphox method, uncertainties stem from sensor noise, sampling frequency, numerical integration, and mass-loading effects. The smartphone accelerometer exhibits intrinsic noise that becomes particularly significant during low-acceleration phases of the motion. Moreover, converting acceleration data into displacement via numerical integration amplifies low-frequency noise and introduces drift, which contributes to uncertainty in identifying oscillation extrema. To mitigate these effects, the oscillation period is extracted using autocorrelation analysis rather than direct peak-to-peak timing. Auto-correlation peak width and repeated measurements estimate period uncertainty, yielding $T = (0.58 \pm 0.01)\ s$.

Phyphox analysis using numerical integration of acceleration amplifies low-frequency noise and can cause baseline drift. To address this, a high-pass filter (≈0.1 Hz cutoff) was applied before integration to remove quasi-static offsets. Linear baseline correction, by subtracting the mean acceleration per cycle, was also implemented. Period determination employed autocorrelation analysis, reducing sensitivity to residual drift compared to peak-to-peak timing. These methods minimize the influence of low-frequency integration artifacts on the oscillation period, ensuring accuracy within uncertainty limits.

The primary source of uncertainty in inertial sensor measurements is the smartphone's added mass, which alters the effective inertial mass and oscillation period. The effective mass is expressed as $m_{eff} = m + m_{phone}$ leading to a corrected theoretical period $T_{theory} = 2\pi\sqrt{\frac{m_{eff}}{k}}$ after accounting for the smartphone mass, the corrected experimental period becomes $T_{eff} = (0.61 \pm 0.01)\ s$, consistent with theoretical expectations within experimental uncertainty. Remaining uncertainty stems from sensor noise, integration drift, and fitting variability.

Comparison of dominant uncertainty sources shows optical tracking minimizes systematic perturbations, yielding smaller relative uncertainties in oscillation period. Inertial sensors, though efficient, introduce significant systematic effects requiring modeling. Stroboscopic imaging's coarse temporal resolution and manual analysis limit it to descriptive assessment[34]. The presented assessment uncertainty analysis offers a consistent framework for interpreting smartphone-based measurement results. By accounting for random and systematic errors, including mass-loading and temporal resolution limits, observed oscillation period differences are explained by physical and instrumental constraints.

4 Conclusion

This research has conducted a controlled evaluation of three smartphone methodologies for assessing simple harmonic motion within a vertical spring-mass configuration. Findings indicate that video analysis offers a dependable quantitative description of oscillatory movement, importantly without introducing mechanical disturbance, thus facilitating precise period measurement under calibrated circumstances. The inertial sensor technique, though convenient, necessitates careful evaluation of mass-loading impacts stemming from the smartphone's own inertia. Once this mechanical effect is accurately adjusted for, the method produces outcomes aligned with theoretical predictions. Conversely, the stroboscopic method's utility is constrained by its temporal resolution and the

inherent subjectivity in manual displacement estimation, thereby limiting its application mainly to qualitative observation of oscillatory dynamics. Collectively, the results underscore the potential of smartphone-based approaches as practical experimental instruments for analyzing SHM, contingent upon the rigorous identification and mitigation of significant uncertainty sources and systematic errors within the experimental design.

References

1 Bhattacharya P, *Advances in Mathematical and Computational Sciences: Proceedings of the ICRTMPCS Intl Conf* , Berlin, Boston: De Gruyter, 1 (2025) pp. 455-460.
2 Garrett S L, *Understanding Acoustics: An Experimentalist's View of Sound and Vibration (Springer)*, 2 (2020) p.p. 59–131.
3 Bocko M F & Onofrio R, *Rev Modern Phys*, 68 (3) (1996) 755.
4 Wang M, Zhang R, Ilic R, Liu Y & Aksyuk V A, *Commun phys*, 4 (1) (2021) 207.
5 Afandi Z, *IOP Conference Series: Mater Sci Eng*, Bristol, 335 (1) (2018) 012064.
6 Adam N C, Leveraging stretchable electronics and IMUs to create a toolbox for measuring in vivo kinetics and kinematics in sheep to facilitate the translation of new medical technologies to humans, ETH Zurich, 29110 (2023) 78.
7 Kuhn J & Vogt P, *Phys Teacher*, 50 (8) (2012) 504.
8 Li D, Liu L & Zhou S, *Phys Teacher*, 58 (9) (2020) 634.
9 Ahmed A A B, Touache A, ElHakimi A & Chamat A, *Phys Educ*, 57 (6) (2022) 065017.
10 Wang Z, Hou Y, Jiang K, Zhang C, Dou W, Huang Z, *et al*., *IEEE Access*. 7 (2019) 100581.
11 Jalal A, Quaid M A K, Tahir S B U D & Kim K, *Sensors*, 20 (22) (2020) 6670.
12 Li Z, Cao L & Jiang S, *IEEE Access*, 11 (2021)40532.
13 Kong X, Yang W, Luo He & Li B, *IEEE Sensors J*, 21 (6) (2021) 8194.
14 Harindranath A & Arora M, *Sensors Actuators A: Phys*, 379 (2024) 115850.
15 Larson Z, Cho Y & Yin X, *Measure Sci Technol*, 28 (6) (2017) 065902.
16 Baker B & Park S, *Phys Teach*, 59 (3) (2021)166.
17 Lahre P, Meshram K, Kumar S, Choubey R K, Kumar R & Patel A K, *Multiscale Multidisciplin Model, Exp Design*, 7 (3) (2024) 2189.
18 El-Sheimy N & Youssef A, *Sat Nav*, 1 (1) (2020) 2.
19 Kuznetsov N, *J Comp Syst Sci Int*, 59 (5) (2020) 647.
20 Mukherjee S & Ganguly S, Real Time Video Analysis using Smart Phone Camera for Stroboscopic Image, Arx, 16 (11) (2016) 1-5.
21 Castañeda-Miranda V H, Luque-Vega L F, Lopez-Neri E, Nava-Pintor J A, Guerrero-Osuna H A & Ornelas-Vargas G, *Sensors*, 21 (18) (2021) 6304.
22 Shen N, Sun Z, Ma H, Xing G, Zhao W, Wang L, *et al*., *Measure*, 70 (1) (2025) 118244.
23 Boimau I & Laos L E. *J Phys Edu Res Stud*, 11 (1) (2024) 21.
24 Konofagou E E & Hynynen K, *Ultrasound Med Bio*, 29 (10) (2003)1405.
25 Tjahjowidodo T, Al-Bender F & Van Brussel H, *Mechatron*, 23 (5) (2013) 497.
26 Huth J, Buchholz M, Kraus J M, Schmucker M, Von Wichert G, Krndija D, *et al*., *BMC cell Bio*, 11 (1) (2010) 24.
27 Luan L, Liu Y & Sun H, *J Sound Vibration*, 565 (2023) 117904.
28 Höpfner H, Morgenthal G, Schirmer M, Naujoks M & Halang C, *ACM SIGMOBILE: Mob Comput Commun Rev*, 17 (4) (2013) 29.
29 Naik M R & Kumar J, *Ind J Pure Appl Phys*, 63 (11) (2025).
30 Handa A, Newcombe R A, Angeli A & Davison A J, *In Eur Conf on Comp Vis Berlin*, Heidelberg: Springer Berlin Heidelberg, 7578 (2012) pp. 222-235.
31 Pan L, Hartley R, Scheerlinck C, Liu M, Yu X & Dai Y, *IEEE Trans Patt Anal Mach Intel*, 44 (5) (2020) 2519.
32 Yu Y, Han S, Chu X, Chu S-I & Wang Z, *Sci*, 296 (5569) (2002) 889.
33 Stubbs C W, *M Notices R Astron Soc*, 508 (3) (2021)3936.
34 Thakkar P, Fleury C, Bainschab M, Sasaki T, Zauner M, Holzmann D, *et al*., *Opt Photon Adv Dimen Metrol II*, SPIE (2022).